Addressing artifacts in PP-PS registration prior to performing joint impedance inversion

Satinder Chopra[1] and Ritesh Kumar Sharma[1]

https://doi.org/10.1190/tle39010047.1

Check for updates

Downloaded 01/14/20 to 192.160.56.248. Redistribution subject to SEG license or copyright; see Terms of Use at http://library.seg.org/

Abstract

Multicomponent seismic data analysis enhances confidence in interpretation by providing mode-converted PS data for imaging the subsurface. Integrated interpretation of PP and PS data begins with the identification of reflections corresponding to similar geologic events on both data sets. This identification is accomplished by carrying out well-log correlation through the generation of PP and PS synthetic seismograms. There are a few issues associated with the approach. One of the issues is that PS data have lower resolution than PP data. This presents difficulties in the correlation of equivalent reflection events on both data sets. Even if few consistent horizons are tracked, the horizon-matching process introduces artifacts on the PS data mapped in PP time. In this paper, we elaborate on such challenges with a data set from the Anadarko Basin in the United States. We then propose a novel workflow to address the challenges.

Introduction

Multicomponent seismic data analysis enhances confidence in interpretation by providing mode-converted PS data for imaging the subsurface. For compressional energy that is incident on a rock interface at an angle different from normal incidence, partitioning takes place in transmitted and reflected compressional (P) and shear (S) components. Mode-converted shear (PS) energy is primarily recorded on the radial component of three-component receivers. Because these waves follow different travel paths with different wavelengths, they "see" the subsurface differently than P-waves. Consequently, PS seismic data exhibit significant changes in amplitude and character of seismic events that may not be seen on PP seismic data. When PP and PS data are analyzed together, more confident interpretation takes place, yielding important rock property estimates such as V_P/V_S. Because V_P values exhibit overlap in different rock types, the added value that V_S brings makes V_P/V_S an important parameter. It was established early on that this ratio is a good lithology indicator (Tatham and Stoffa, 1976; Tatham, 1982; Pardus et al., 1990), is good at identifying limestone/shale boundaries (Goldberg and Gant, 1988) and sand/shale ratios in channels (Garotta et al., 1985), and is sensitive to fluids (Dillon et al., 2003) and porosity (Pigott et al., 1990). Such applications have continued to be demonstrated in the literature, but it is important to note that they can only be successful if the determined values of V_P/V_S are accurate.

Conventional vertical-component seismic data allow the estimation of mode-converted shear at oblique angles of incidence, which after simultaneous inversion, yields V_P/V_S. Multicomponent seismic data provide the actual recorded horizontal radial component, which is what we refer to as "PS data." PS data are expected to provide significant information to PP seismic data interpretation, but the differences in timescales prevent an easy visual comparison between them. To accomplish this, PS data are converted to PP two-way traveltime. Once this is done, not only can the coupled interpretation of PP and PS data be carried out, but both types of data can be put through an integrated or joint impedance inversion, yielding V_P/V_S data.

Integrated interpretation of PP and PS data begins with the identification of reflections corresponding to similar geologic events on both data sets. This identification is accomplished by carrying out well-log correlation through the generation of PP and PS synthetic seismograms. If check shots or vertical seismic profile data are not available, slight stretching/squeezing may be necessary. One way to generate a PS synthetic seismogram is to use V_S and density curves to generate a PS elastic gather with a wavelet extracted from PS stacked data and then stack it. The stacked gather trace can be correlated with the PS stacked data. The other method is to generate angle-dependent PS reflectivity at 10° or 12° and use it to generate the PS synthetic seismogram. It is assumed here that a shear sonic curve is available, and both synthetic seismograms are generated over the same range of frequency bandwidth as the input seismic reflection data.

Such a correlation helps with the visual identification of events on PS sections at the location of the well, considering their character, relative amplitudes, and approximate traveltimes. In a similar way, reflection events are identified on PP data. When the events of interest are identified and correlated on the PP and PS sections (through respective synthetic seismograms) at the location of the wells, horizons are picked on the data volumes on an interpretation workstation. The peak amplitude on the PP and PS data represents an increase in elastic impedance across the interface that it is representing. Mis-ties may be seen on such synthetic-seismic correlations, and one should keep an open mind while analyzing the reasons.

While performing event correlations between PP and PS data, a peak on PP data is expected to correlate with an equivalent peak on PS data. However, this is not always the case (e.g., the oil sands area in northern Alberta, Canada, where the Paleozoic marker is a difficult pick). The Paleozoic marker is a weathered unconformity between the Paleozoic carbonates and Cretaceous clastics. The relative compressibility and rigidity of the weathered carbonates as well as the tuning artifacts make the seismic response exhibit a peak at places, which becomes a zero crossing or a trough at others (Anderson and Larson, 2006). In such cases, a prominent horizon above or below can be used for horizon picking.

Next, the equivalent correlative events on the PP and PS data volumes are used to map or shrink the PS timescale to the PP timescale, a process referred to as "registration." This step has

[1]TGS, Calgary, Alberta, Canada. E-mail: satinder.chopra@tgs.com; ritesh.sharma@tgs.com.

Downloaded 01/14/20 to 192.160.56.248. Redistribution subject to SEG license or copyright; see Terms of Use at http://library.seg.org/

complications including difficulty in picking horizons in areas with complicated geology, faulting, etc.; one or more peaks on PP data corresponding to a trough on PS data; and lower frequency content of PS data than PP data due to different attenuations suffered by component frequencies during wave propagation. Some automated methods based on warping one data set with the other have been introduced (Herrera and van der Baan, 2012; Hale, 2013; Compton and Hale, 2014; Gao and Sacchi, 2018). However, in the absence of adequate software for such methods, the earlier-mentioned manual registration exercise can be used. Excessive care is required while performing this step because any artifact(s) introduced will show up on the joint impedance inversion and lead to incorrect interpretation. The earlier artifacts are applicable to a data set from the Anadarko Basin in Oklahoma, and we present a workflow to address them.

Artifacts resulting from application of a conventional workflow

In Figure 1, we show the well-to-seismic correlation for PS data. The well-log curves (V_P, V_S, and rho) are shown in Figure 1a. The PS synthetic seismogram (blue) correlation with real PS seismic data (red) is shown in Figure 1b. A segment of the PS section (in PS time) is shown in Figure 1c. An equivalent segment of PP data (in PS time) is shown in Figure 1d. The correlation between the PS synthetic and seismic data was found to be 84%, which is reasonably good. As stated earlier, once the well-to-seismic correlation for PP and PS seismic data is satisfactory, horizon picking is carried out to map all trackable horizons on PS data that are equivalent to those picked on PP data. The depth-time curves for PP and PS data are determined at the well location to estimate V_P/V_S in different intervals. The estimated interval V_P/V_S at the well is propagated over 3D seismic data to obtain an initial V_P/V_S volume, which is used to transform PS data from its original time domain to PP time domain. Had it been valid everywhere, a perfect match between PP and PS horizons would have been noticed. However, a mismatch between the two types of horizons, except at the well location, is generally noticed (Figures 2a and 2b). Geologically, such a mismatch is not acceptable because a geologic marker would be expected at the same time on both of the data sets after registration. The discrepancies show up because the interval V_P/V_S is only valid at the well location and may not be valid at other lateral locations.

We try to match the picked horizons on PP and PS data to make them geologically consistent. Residual V_P/V_S values used in the domain conversion can be estimated by using the PP and PS isochrons in the following equation (Garotta et al., 1985):

$$\frac{V_P}{V_S} = 2\left(\frac{PS\ isochron}{PP\ isochron}\right) - 1\,. \tag{1}$$

The V_P/V_S values computed at every trace are compared with the initial V_P/V_S volume. The observed differences in V_P/V_S are

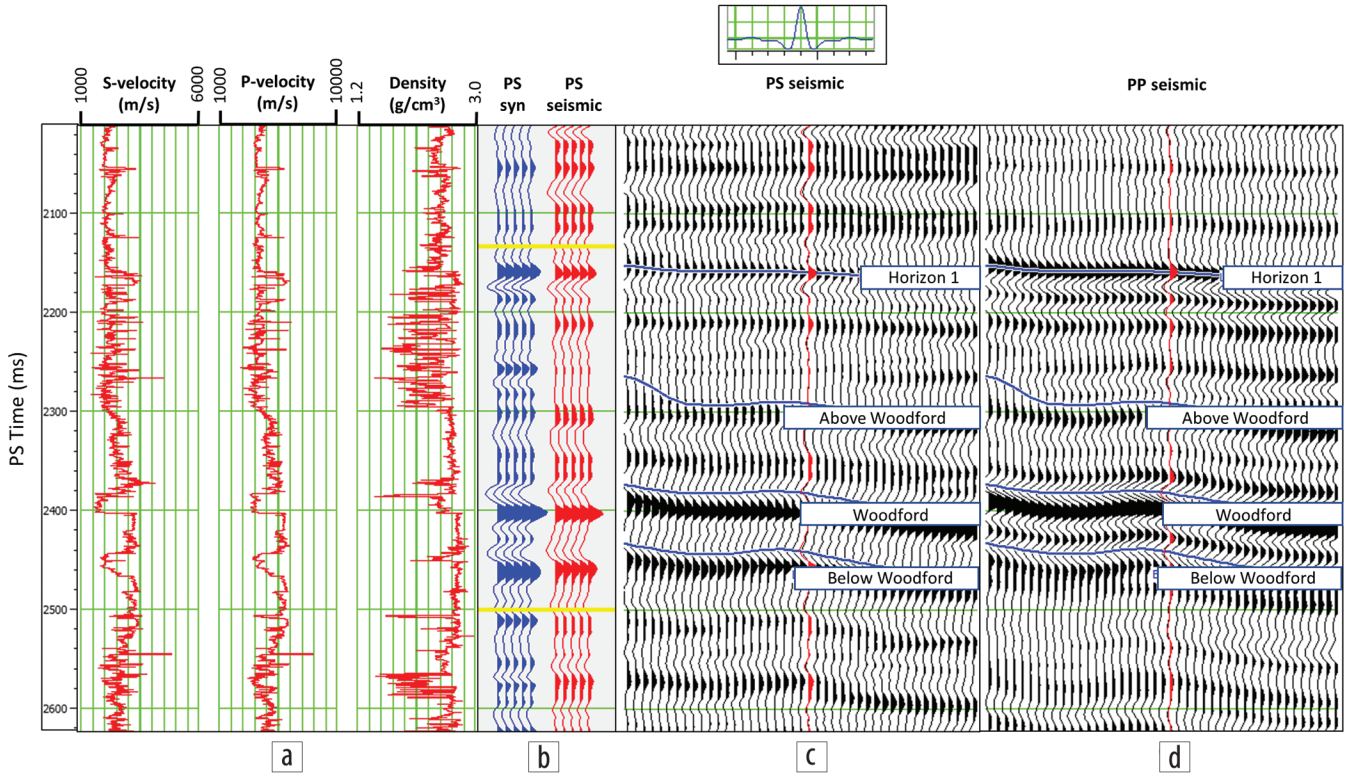

Figure 1. Well-to-seismic correlation for PS data and registration with PP data at the location of a well. (b) The PS synthetic seismogram (blue) correlated with PS real seismic traces (red). The displayed wavelet, used for the generation of the synthetic seismogram, was extracted from PS seismic data using a statistical process. Good correlation (84%) is seen between the synthetic and real traces. The (c) PS and (d) PP data are shown in PS time. (Data courtesy of TGS, Houston)

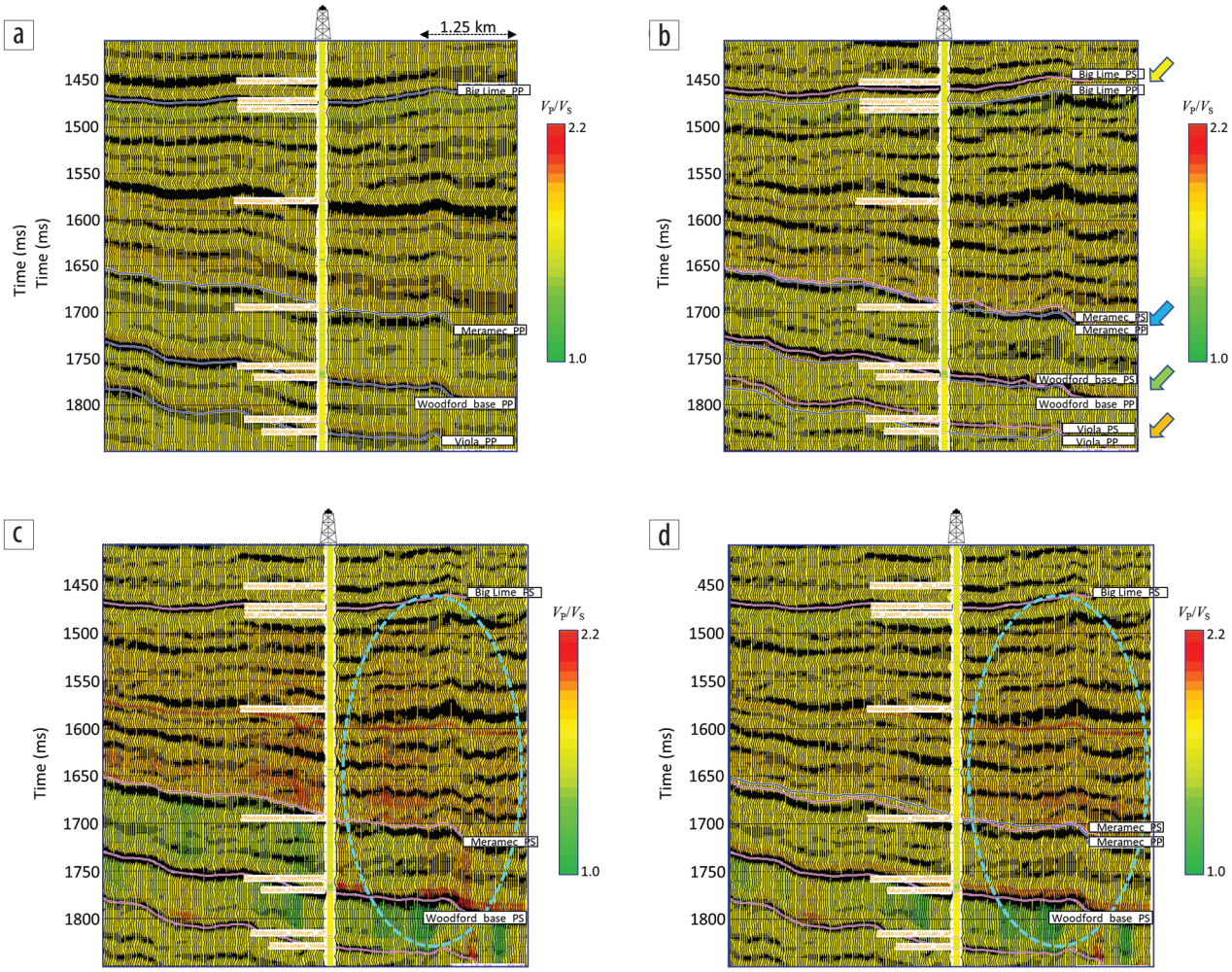

Figure 2. Segments of seismic sections from (a) PP and (b) PS data in PP time. Four equivalent reflection events have been picked on the data volumes (colored arrows), but horizon matching has not yet been done. The V_P/V_S values at every CDP are overlaid in color. (c) The same PS section as in (b), but with horizons matched. Notice the revised values of V_P/V_S, which seem uneven (red and green) and not correlated with the well-log curve. Also, notice the reflection distortions in the form of undulations within the cyan ellipse. (d) The same section as in (c), but skipping matching of the Meramec horizons during horizon matching. The distortion in the reflections is minimized, and the V_P/V_S values seem to be better distributed. (Data courtesy of TGS, Houston)

distributed within the intervals at every common-midpoint location, resulting in time shifts of reflection events.

While this process solves the horizon mismatch problem at various intervals bounded by horizons, some artifacts are seen within the intervals (Figure 2c). Figure 2c shows an equivalent PS section in PP time with V_P/V_S overlay. The revised values are shown in color, which exhibit an uneven distribution. Some of the reflections are also seen as having undulations (cyan ellipse). One could attempt to avoid matching the Meramec horizons in between the Big Lime and Woodford markers, which tends to better distribute the V_P/V_S values (Figure 2d). The jitter in the seismic reflections (indicated within the cyan ellipse in Figure 2c) is also minimized. Thus, it seems that the problem is alleviated. However, this may not happen every time skipping an intermediate horizon is attempted. We consider such observations as artifacts. If these artifacts are not corrected properly before performing prestack joint impedance inversion, they could degrade the results.

Besides this important issue, there is a significant difference in the PP and PS spectral bandwidth after registration. This is found to be generally true and again results in the degradation of the prestack joint inversion performance. Figure 3a shows a frequency spectra comparison of the wavelets extracted from PP and PS data in PP time.

Attempts to address artifacts

A workflow has been created to address the earlier-mentioned artifacts (Figure 4). After performing well-to-seismic correlations for PP and PS seismic data and using the picked horizons bounding the broad zone of interest, the PS data are transformed into PP two-way traveltime. Next, frequency spectra balancing of PS data is carried out. The method adopted for spectral flattening by balancing the power (square of the spectral magnitude) was first discussed by Marfurt and Matos (2014). It makes use of the average power spectrum at a given time as well as the average spectral magnitude. Because a single time-varying spectral balancing operator is applied to each trace, this spectral balancing approach is considered to be amplitude friendly (Chopra and Marfurt, 2016). In Figure 3b, we show the frequency spectra and wavelets for PP and PS spectrally balanced data in PP time. The flattened frequency spectra of PP and PS data are well noticed. Because PP and PS data could have

Downloaded 01/14/20 to 192.160.56.248. Redistribution subject to SEG license or copyright; see Terms of Use at http://library.seg.org/

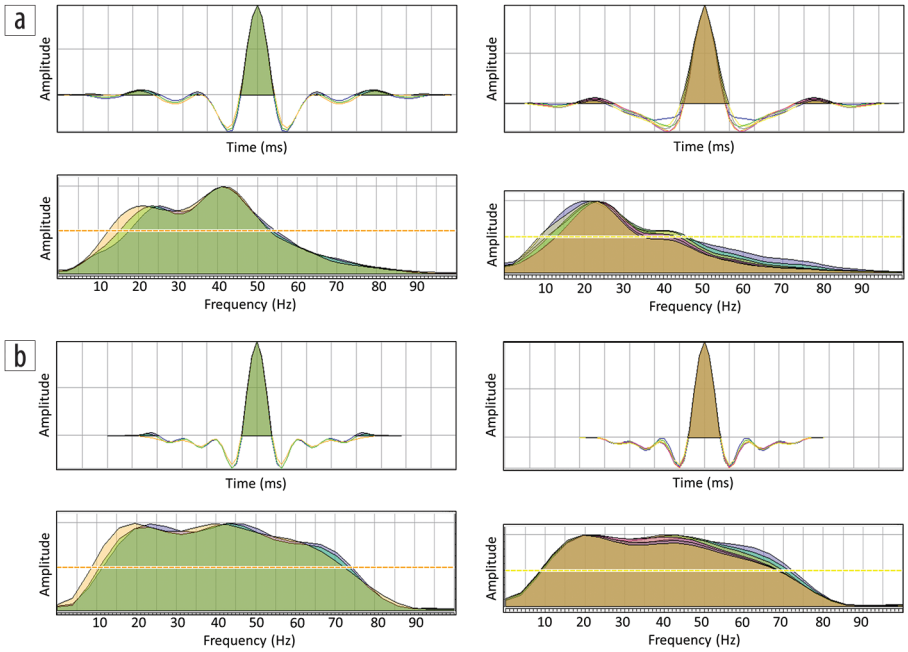

Figure 3. Wavelets and their frequency spectra extracted from (left) PP (three angle stacks: 1°–14°, 14°–26°, 26°–39°) and (right) PS (five angle stacks: 7°–16°, 16°–26°, 26°–35°, 35°–44°, 44°–54°) data in PP time (a) before and (b) after spectral balancing. The frequency content of PS data, which is appreciably lower than PP data, is significantly improved after balancing.

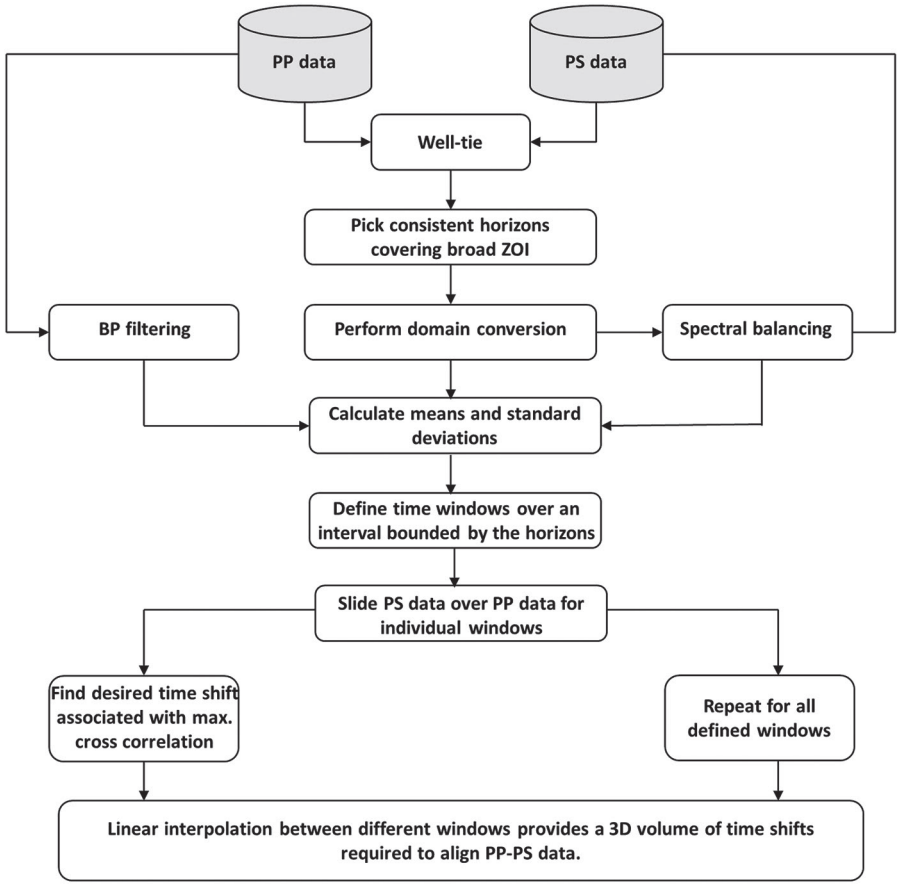

Figure 4. The proposed workflow.

different amplitude levels, the next step normalizes the two data sets by using z-transformation, which requires computation of the mean and standard deviation. By using the picked horizons, stratal intervals are defined over the broad zone of interest on PP and PS data and are crosscorrelated to find time shifts for maximum correlation. Such time shifts are linearly interpolated to produce a volume of time shifts that align PP and PS seismic data.

Figure 5a shows an S-impedance section obtained from prestack joint impedance inversion before using the proposed workflow. The equivalent section after using the proposed workflow is shown in Figure 5b. Notice the clearer definition of the event (cyan arrows).

Similarly, in Figure 6 we show V_P/V_S-equivalent arbitrary line sections drawn from V_P/V_S volumes obtained by prestack joint impedance inversion before and after the proposed workflow. Notice the overall better resolution in Figure 6b.

We show a comparison of crossplots between P-impedance and V_P/V_S generated from well data (Figure 7a) as well as the inverted data before (Figure 7b) and after (Figure 7c) the proposed workflow. Not only are the overall clusters of inverted data following the trend seen for the well data, but the cluster points corresponding to low V_P/V_S and low impedance better separate after balancing (ellipses). This separation has an important implication. When cluster points are back-projected on the vertical seismic sections, they better illuminate the sweet spots.

Conclusions

In this study, attention has been drawn to a couple of important issues that appear while performing registration of multicomponent PS and PP seismic data before the data are taken into prestack joint impedance inversion. These issues include generation of uneven or abnormal V_P/V_S values in different intervals as well as lower frequency content of PS data after domain conversion to PP two-way traveltime. If such issues are left unaddressed, they lead to artifacts in the prestack joint

Downloaded 01/14/20 to 192.160.56.248. Redistribution subject to SEG license or copyright; see Terms of Use at http://library.seg.org/

Downloaded 01/14/20 to 192.160.56.248. Redistribution subject to SEG license or copyright; see Terms of Use at http://library.seg.org/

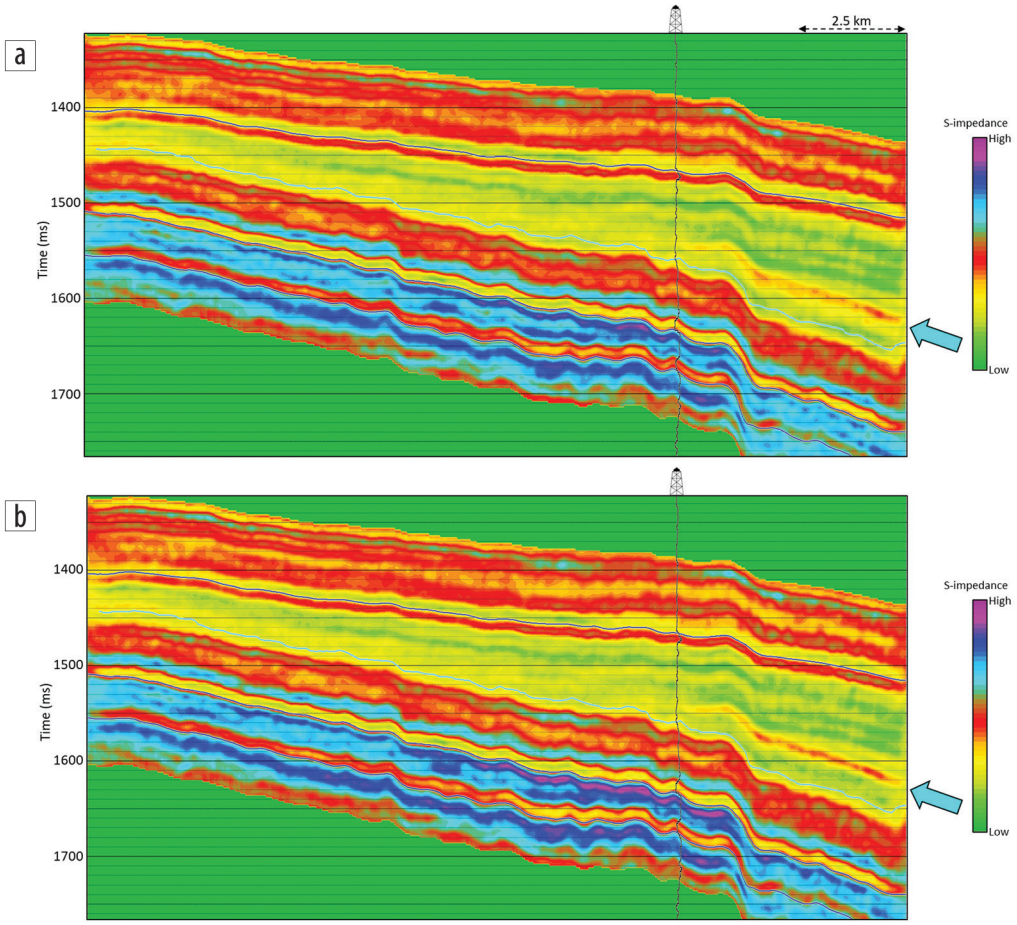

Figure 5. Segments of S-impedance sections obtained from prestack joint impedance inversion (a) before and (b) after spectral balancing of PS seismic data in PP time. Notice the stronger definition of the event (cyan arrow).

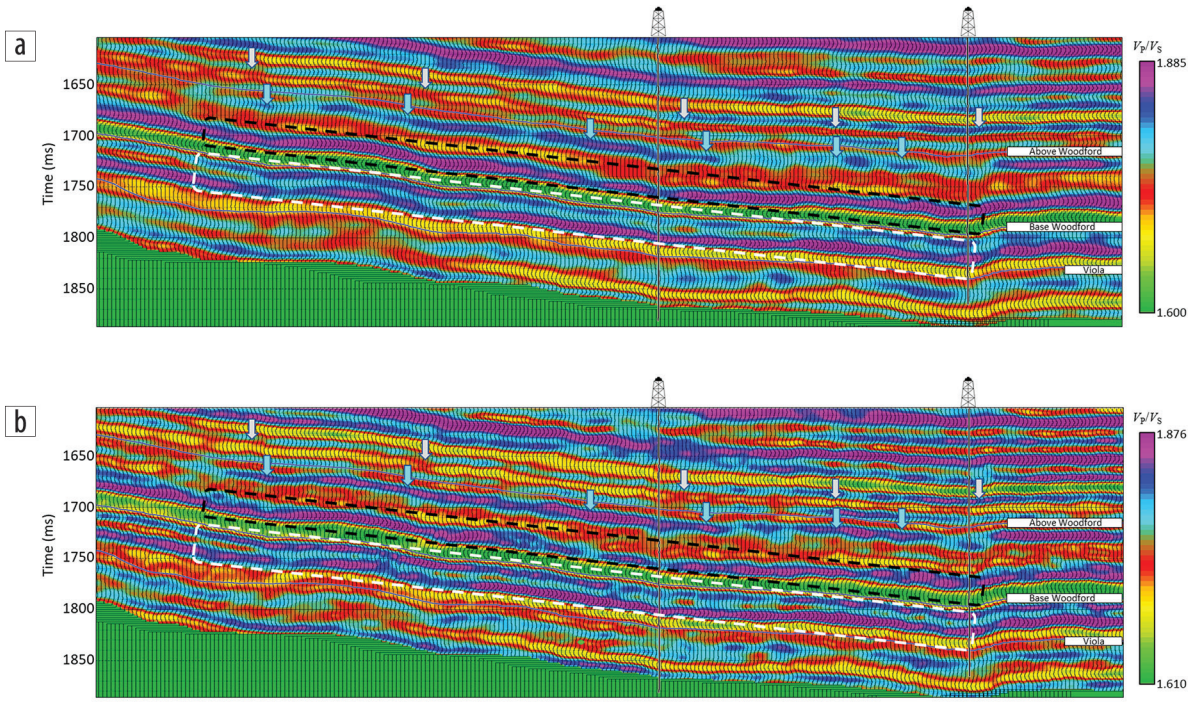

Figure 6. An arbitrary line passing through two wells from the V_P/V_S volume generated by using prestack joint impedance inversion (a) before and (b) after balancing. Notice the overall better resolution in the different intervals after spectral balancing. (Data courtesy of TGS, Houston)

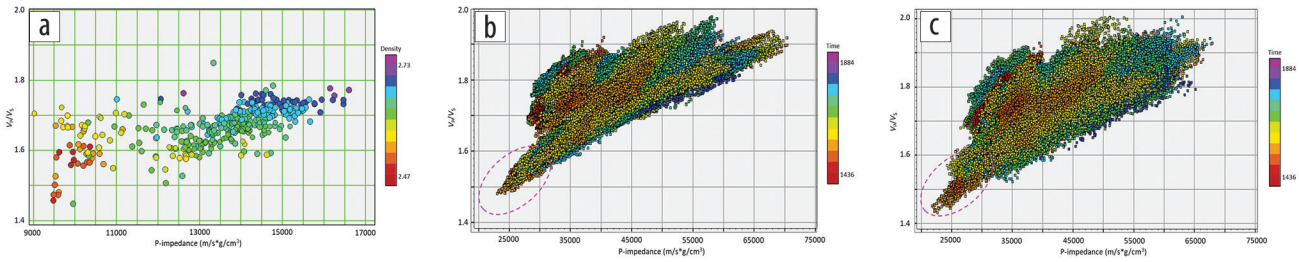

Figure 7. Crossplot between P-impedance and V_P/V_S, color coded with density from well data between the Meramec and base of the Woodford interval. Equivalent crossplots generated using prestack joint inversion (b) before and (c) after spectral balancing, color coded with time for the same interval. Not only is the overall cluster of inverted data following the trend seen for the well data, but the cluster points corresponding to low V_P/V_S and low impedance separate after balancing (ellipse).

impedance inversion carried out for the generation of elastic parameters. We have devised a workflow that addresses the issues and produces results that are free of artifacts, leading to superior and more meaningful results. TLE

Acknowledgments

We thank TGS for encouraging this work and for permission to present and publish it. The well data used were obtained from the TGS Well Data Library.

Data and materials availability

Data associated with this research are confidential and cannot be released.

Corresponding author: satinder.chopra@tgs.com

References

Anderson, P., and R. Larson, 2006, Multicomponent case study: One company's experience in eastern Alberta: CSEG Recorder, **31**, no. 9, 5–10.

Chopra, S., and K. J. Marfurt, 2016, Spectral decomposition and spectral balancing of seismic data: The Leading Edge, **35**, no. 2, 176–179, https://doi.org/10.1190/tle35020176.1.

Compton, S., and D. Hale, 2014, Estimating V_P/V_S ratios using smooth dynamic image warping: Geophysics, **79**, no. 6, V201–V215, https://doi.org/10.1190/geo2014-0022.1.

Dillon, L., G. Schwedersky, G. Vásquez, R. Velloso, and C. Nunes, 2003, A multiscale DHI elastic attributes evaluation: The Leading Edge, **22**, no. 10, 1024–1029, https://doi.org/10.1190/1.1623644.

Gao, W., and M. D. Sacchi, 2018, Multicomponent seismic data registration by nonlinear optimization: Geophysics, **83**, no. 1, V1–V10, https://doi.org/10.1190/geo2017-0105.1.

Garotta, R., P. Marechal, and M. Megesan, 1985, Two-component acquisition as a routine procedure for recording P-waves and converted waves: Canadian Journal of Exploration Geophysics, **21**, no. 1, 40–53.

Goldberg, D., and W. T. Gant, 1988, Shear-wave processing of sonic log waveforms in a limestone reservoir: Geophysics, **53**, no. 5, 668–676, https://doi.org/10.1190/1.1442501.

Hale, D., 2013, Dynamic warping of seismic images: Geophysics, **78**, no. 2, S105–S115, https://doi.org/10.1190/geo2012-0327.1.

Herrera, R. H., and M. van der Baan, 2012, Guided seismic-to-well tying based on dynamic time warping: 82nd Annual International Meeting, SEG, Expanded Abstracts, https://doi.org/10.1190/segam2012-0712.1.

Marfurt, K., and M. Matos, 2014, Am I blue? Finding the right (spectral) balance: AAPG Explorer, https://explorer.aapg.org/story/articleid/9522/am-i-blue-finding-the-right-spectral-balance, accessed 21 November 2019.

Pardus, Y. C., J. Conner, N. R. Schuler, and R. H. Tatham, 1990, V_P/V_S and lithology in carbonate rocks: A case study in the Scipio Trend in southern Michigan: 60th Annual International Meeting, SEG, Expanded Abstracts, 169–172, https://doi.org/10.1190/1.1890101.

Pigott, J. D., R. K. Shrestha, and R. A. Warwick, 1990, Direct determination of carbonate porosity and pressure from AVO inversion: 60th Annual International Meeting, SEG, Expanded Abstracts, https://doi.org/10.1190/1.1890047.

Tatham, R. H., 1982, V_P/V_S and lithology: Geophysics, **47**, no. 3, 336–344, https://doi.org/10.1190/1.1441339.

Tatham, R. H., and P. L. Stoffa, 1976, V_P/V_S — A potential hydrocarbon indicator: Geophysics, **41**, no. 5, 837–849, https://doi.org/10.1190/1.1440668.

Downloaded 01/14/20 to 192.160.56.248. Redistribution subject to SEG license or copyright; see Terms of Use at http://library.seg.org/